Applied Surface Science 276 (2013) 543–549

Contents lists available at SciVerse ScienceDirect

Applied Surface Science

journal homepage: www.elsevier.com/locate/apsusc

Surface morphology, cohesive and adhesive properties of amorphous hydrogenated carbon nanocomposite films

A. Lazauskas [a,*], V. Grigaliūnas [a,1], Š. Meškinis [a,1], F. Ecarla [b,2], J. Baltrusaitis [c,3]

[a] Institute of Material Science, Kaunas University of Technology, Savanorių 271, 3009 Kaunas, Lithuania
[b] CSM Instruments SA, Rue de la Gare 4, 2034 Peseux, Switzerland
[c] PhotoCatalytic Synthesis Group, MESA+ Institute for Nanotechnology, Faculty of Science and Technology, University of Twente, Meander 229, P.O. Box 217, 7500 AE Enschede, The Netherlands

ARTICLE INFO

Article history:
Received 16 October 2012
Received in revised form 19 March 2013
Accepted 20 March 2013
Available online 28 March 2013

Keywords:
Amorphous hydrogenated carbon
Thin film
AFM
Scratch test
XPS

ABSTRACT

In this work, amorphous hydrogenated carbon (a-C:H), SiO_x containing a-C:H (a-C:H/SiO_x) and nitrogen-doped a-C:H/SiO_x (a-C:H:N/SiO_x) thin films were deposited on chromium thin film coated glass using a closed drift ion beam source. Acetylene gas, hexamethyldisiloxane and hydrogen or 20% nitrogen/hydrogen mixture were used as precursors. Resulting hydrogenated carbon thin film surface morphology as well as their cohesive and adhesive properties were studied using progressive loading scratch tests followed by optical microscopy analysis. Surface analysis was also performed using atomic force microscopy via topography, surface morphology parameter, height distribution histogram and bearing ratio curve based hybrid parameter measurements. The a-C:H/SiO_x and a-C:H:N/SiO_x thin films showed better mechanical strength as compared to the conventional a-C:H films. X-ray photoelectron spectroscopy was used to determine the chemical composition of these films. It showed increased amounts of silicon and absence of terminal oxygenated carbon bonds in a-C:H:N/SiO_x thin film which was attributed to its improved mechanical properties.

1. Introduction

Diamond-like carbon (DLC) belongs to a metastable phase of carbon, which has a random network of covalently bonded carbon in sp^3 and sp^2 local coordination, with some of the bonds terminated by H [1]. DLC films can be divided into two broad categories based on their structure: amorphous carbon and hydrogenated amorphous carbon (a-C:H) both having a high fraction of metastable sp^3 carbon bonds which determine the "diamond-like" structure of the DLC films [2]. The amorphous nature of DLC opens up the possibility of incorporating other elements such as Si, F, P, Ag and N [3–6] which can result in a new or improved functionality of the material. Depending on the sp^3 (diamond-like) and sp^2 (graphite-like) bond content, hydrogen and other incorporated element concentration, DLC physical properties could be altered to obtain friction and wear reduction [7,8], biocompatibility, hemocompatibility, prevention of metal ion release [9–11], exceptional optical transmission and antireflection [12,13] functionality of the materials. Commonly used DLC deposition techniques include filtered cathodic arc, plasma enhanced chemical vapor deposition, direct ion beam (IB), electron cyclotron resonance plasma chemical vapor deposition and DC/RF sputtering [14–17]. IB deposition in particular has some advantages over the other methods of hydrogenated amorphous carbon film synthesis. Parameters of the film growth process such as ion beam energy, plasma power, substrate temperature, system pressure, gas composition can be precisely controlled over a wide range of conditions. DLC films can be deposited onto electrically conductive and insulating materials providing flexibility that one needs in designing and developing multifunctional films [18,19]. However, DLC films exhibit some undesirable properties such as high compressive residual stress, which arise due to the energetic deposition processes of these films. The residual stress may cause mechanical instability of the DLC resulting in adhesion failures and delamination of the films from the substrate surface. The elimination and release of residual stress may also be the cause of the undesirable morphological and microstructural changes of the films [20]. As a result, there is considerable interest in developing synthesis and surface treatment approaches oriented toward enhancing the adhesive performance of DLC films. A common practice is to use a metallic interlayer deposited between the substrate surface and the DLC film; for instance chromium (Cr),

* Corresponding author. Tel.: +370 671 73375; fax: +370 37 314423.
E-mail addresses: Algirdas.LAZAUSKAS@stud.ktu.lt (A. Lazauskas), Viktoras.GRIGALIUNAS@ktu.lt (V. Grigaliūnas), Sarunas.MESKINIS@ktu.lt (Š. Meškinis), Fanny.ECARLA@csm-instruments.com (F. Ecarla), j.baltrusaitis@utwente.nl (J. Baltrusaitis).
[1] Tel.: +370 37 31 3432; fax: +370 37 314423.
[2] Tel: +41 32 557 56 18; fax: +41 32 557 56 10.
[3] Tel.: +31 53 489 3968; fax: +31 53 489 2882.

0169-4332/$ – see front matter © 2013 Elsevier B.V. All rights reserved.
http://dx.doi.org/10.1016/j.apsusc.2013.03.131

titanium, tungsten, or silicon [21]. Other methods include plasmochemical treatment of the substrate surface, doping of DLC itself or a combination [22] of these.

In this study, we report on the synthesis and surface morphological, adhesive and cohesive characterization of a-C:H, SiO_x containing a-C:H (a-C:H/SiO_x) and nitrogen-doped a-C:H/SiO_x (a-C:H:N/SiO_x) films deposited on Cr/glass substrates using a closed drift ion beam source. In all measurements, Cr was used as an interlayer to enhance the adhesion between the soda–lime–silica float glass substrate (denoted as Cr/glass templates) and DLC films. Surface morphology of these films is related to their mechanical behavior thus also contributing to the film-to-substrate adhesive bonding strength and cohesive properties. Surface morphology parameters, height distribution histograms and bearing ratio curve quantification were obtained using atomic force microscopy (AFM) topographical imaging. Cohesive and adhesive properties of the synthesized films were evaluated using scratch test progressive loading followed by optical microscopy inspection. AFM was also utilized to measure critical sections of a scratch track and to accurately determine the wear mechanism of films after the scratch. Finally, elemental analysis was performed using X-ray photoelectron spectroscopy (XPS) to obtain possible surface chemical composition-thin film mechanical property relationships.

2. Experimental technique

2.1. Thin DLC film production

A commercial soda–lime–silica float glass (Pilkington NSG Group Flat Glass Business) of thickness 1 mm was used in this study. Glass was cut into 1.5 cm × 1.5 cm slides. Surface preparation included RCA-1 cleaning. For quality testing of glass substrate surface hydrophilic properties, contact angle measurements were performed at room temperature (20 °C) by the sessile drop method and contact angle measured using method based on B-spline snakes (active contours) [23]. Measurements of contact angles were taken within 10 s after formation of the sessile drop. As expected, prepared glass surfaces were free of any hydrophobic contaminants with low contact angles ranging from 5° to 10°.

Chromium thin film deposition was performed using a two-step thermal evaporation technique. Details of the deposition technique, conditions and characteristic surface morphology of the films can be found elsewhere [24]. Briefly, a two-step thermal evaporation technique was used and the thickness of the deposited thin Cr multilayer composite films was 80 nm.

The Hall-type closed drift ion beam source was used to deposit a-C:H, a-C:H/SiO_x and a-C:H:N/SiO_x films at room temperature. The base pressure was 2×10^{-4} Pa, work pressure $1–2 \times 10^{-2}$ Pa, and constant ion beam energy of 500 eV was applied with current density of 0.06 mA/cm^2. Low energy beam was shown before to yield well defined thin DLC films [19,25]. Three precursor gases were used: acetylene (C_2H_2) for synthesis of a-C:H films; hexamethyldisiloxane (HMDSO) ($(CH_3)_3SiOSi(CH_3)_3$) with H_2 transport gas for synthesis of a-C:H/SiO_x films; and HMDSO with 20% N_2/H_2 transport gas mixture for synthesis of a-C:H:N/SiO_x films. Control tests with monocrystalline Si(1 0 0) samples were carried out to determine deposition rates for all three carrier gases. The thickness of the control samples was determined using He–Ne laser (k = 632.8 nm) laser ellipsometer (Gaertner L-115). Film thickness of 200 nm according to the evaluated control deposition rates [19] was chosen for the deposition of DLC films on Cr/glass substrates.

2.2. AFM measurements and scratch tests

AFM experiments were carried out in air at room temperature using a Microtestmachines NT-206 atomic force microscope, while data was analyzed using SurfaceView scanning probe microscopy data processing software. Topographical images were collected using a V-shaped silicon cantilever (spring constant of 3 N/m, tip curvature radius of 10.0 nm and the cone angle of 20°) operating in the contact image mode with 4 μm × 4 μm scan size.

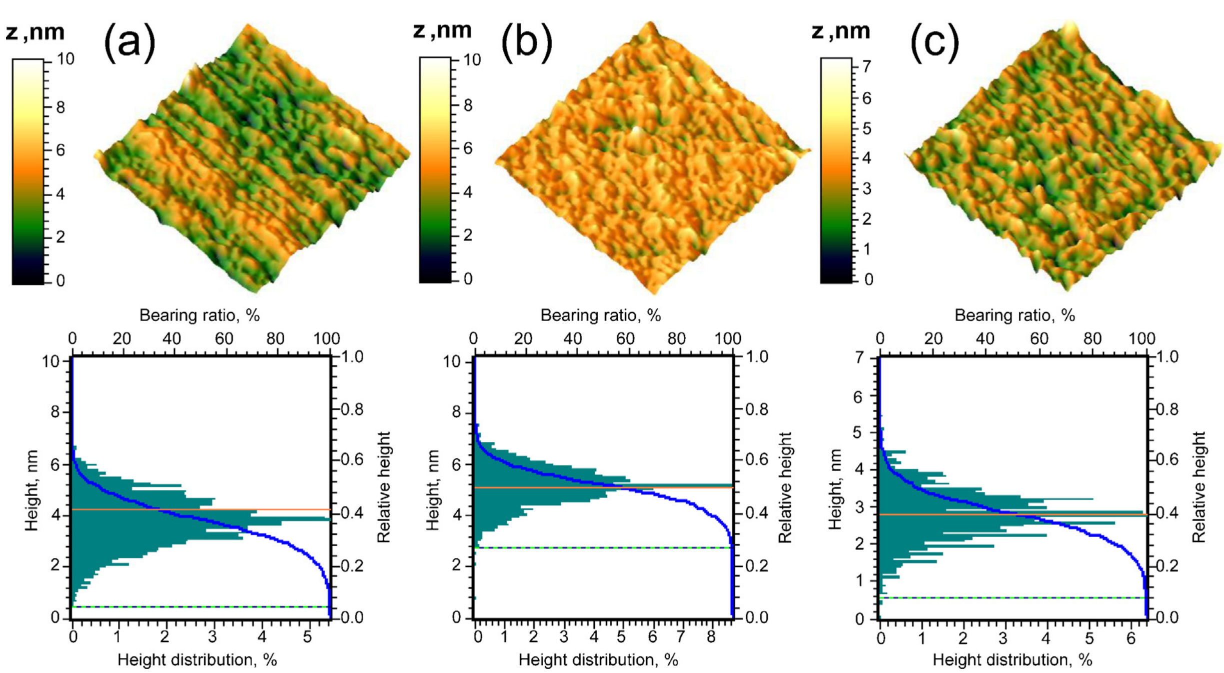

Fig. 1. (*Top*) Characteristic 4 μm × 4 μm AFM 3D topographical images with normalized z axis in nm as well as (*bottom*) normalized height distribution histograms and bearing ratio curves of (a) a-C:H:N/SiO_x film surface, (b) a-C:H film surface and (c) a-C:H/SiO_x film surface. Dashed horizontal line in height distribution histogram indicates the height at which surface structures are connected to each other. The solid horizontal line indicates the mean height.

Table 1
Summary of surface morphology parameters.

Sample	Parameters						
	R_q (nm)	Z_{mean} (nm)	R_{sk}	R_{ku}	R_k (nm)	R_{pk} (nm)	R_{vk} (nm)
a-C:H:N/SiO_x	1.04	3.80	0.03	4.05	2.60	0.80	1.10
a-C:H	0.84	5.17	−0.19	5.45	1.90	1.20	0.80
a-C:H/SiO_x	0.73	2.82	0.13	4.38	1.80	0.95	0.70

Surface morphology was evaluated using AFM surface topography images. In particular, roughness parameters – root mean square (RMS) roughness (R_q), skewness (R_{sk}) and kurtosis (R_{ku}), height distribution histograms and bearing ratio curves were used.

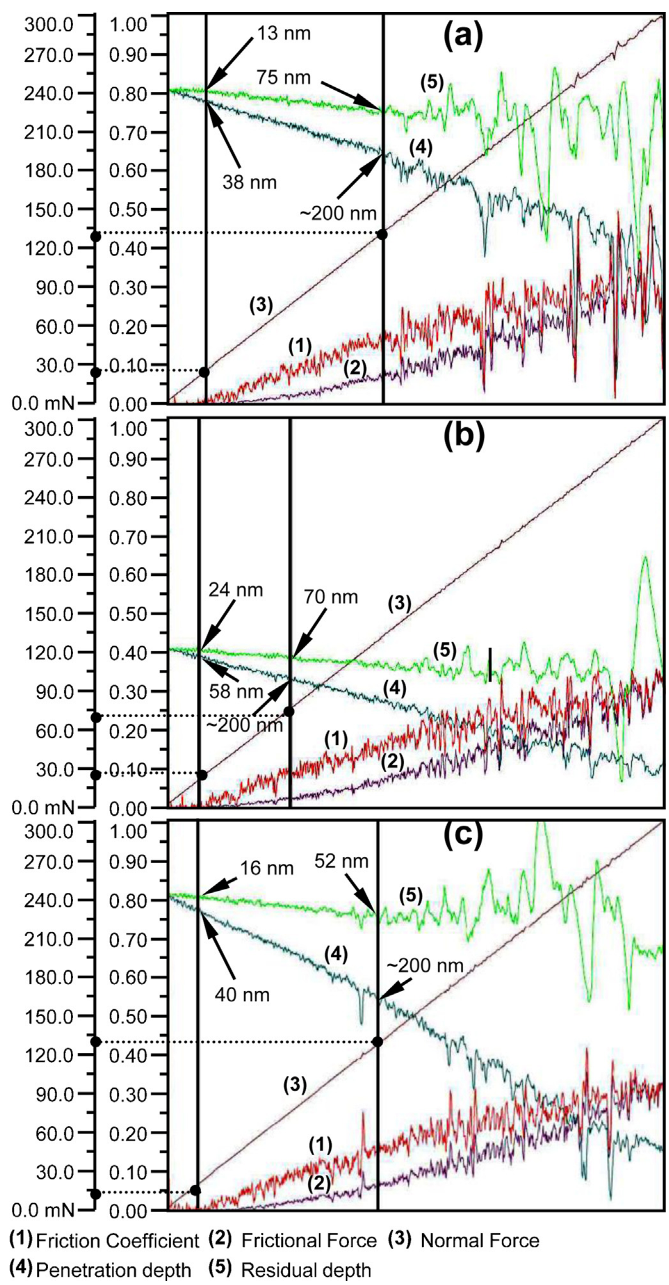

Fig. 2. Scratch test data for (a) a-C:H:N/SiO_x, (b) a-C:H and (c) a-C:H/SiO_x films. Friction coefficient (1), frictional force (2), normal force (3), penetration depth (4) and residual depth (5) characteristic resulting curves as a function of the scratch length are shown. First vertical axis (from right to left) corresponds to the friction coefficient and the second axis to frictional force and normal force. Arrows indicate the penetration depth and residual depth at the critical loads. Dotted horizontal lines indicate values of critical loads.

RMS roughness is the average of measured height deviations taken within the evaluation area and measured from the mean linear surface. Skewness parameter indicates surface symmetry within the evaluation area. Negative skewness indicates predominance of valleys and with a positive value indicating a surface having more peaks. Kurtosis is a measure of the randomness of heights, as well as the sharpness of a surface. For a Gaussian-like surface it has a value of 3 [26]. The farther the result is from 3, the less random and more repetitive the surface is. Height distribution histograms show the share of the surface points located at a given height relative to the total number of surface points in percent. Bearing ratio curve is defined as the dependence of the solid material occurrence on the feature height. To obtain more detailed information about morphology of the surfaces, we defined hybrid parameters of the bearing ratio curve by dividing it into three regions [27]. The upper region of the bearing ratio curve indicates the portion of the surface structures (i.e. peaks) which would be first affected during the contact with another surface and is defined as reduced peak height, R_{pk}. The middle region of the bearing ratio curve indicates the portion of the surface structures responsible for the stiffness characteristics, performance and life of the surface during wear and is defined as core-roughness, R_k. The lower region of bearing ratio curves exhibits surface structures (i.e. valleys) where water molecules adsorbed from the atmosphere could condense or air gaps between the contacting surfaces could emerge affecting the surface adhesive properties, as well as their frictional performance and is defined as reduced valley depth, R_{vk}.

The adherence of the DLC films was measured using a CSM Nano Scratch Tester. During the scratch test, the synthesized DLC films were scratched (scratch length 2 mm and speed 4 mm/min) with a sphero-conical stylus (cone angle 90° and indenter radius 5 μm) applying progressive loading (initial load of 3 mN and final load of 300 mN) at a fixed rate (loading rate 594 mN/min). The scratches were performed in air (temperature 23 °C and humidity 40%). The displacement of the indenter, normal force and the occurring tangential (frictional) force were recorded. Optical microscopy inspection was used to detect coating failure after scratching and differentiate between the cohesive failure within the coating and adhesive failure at the interface of the DLC/Cr system. The scratch resistance of the DLC films and the adhesion to the Cr films were evaluated by comparing critical load (L_{c1}), e.g. the load at which the first crack or failure appears on the film and another critical load (L_{c2}), the load at which the full delamination of the film occurs [28]. Three scratches were performed for each sample and mean values of L_{c1} and L_{c2} were calculated. A more detailed analysis of the critical sections of a scratch track was performed using AFM topographical images (12 μm × 12 μm scan size) and length profiles of the scratch tracks.

2.3. XPS measurements

XPS was performed using a Kratos Axis Ultra DLD spectrometer. The surface analysis chamber is equipped with monochromatic radiation at 1486.6 eV from an aluminum K_α source using a 500 mm Rowland circle silicon single crystal monochromator. The X-ray gun was operated using a 15 mA emission current at an accelerating voltage of 15 kV. Low energy electrons were used for charge

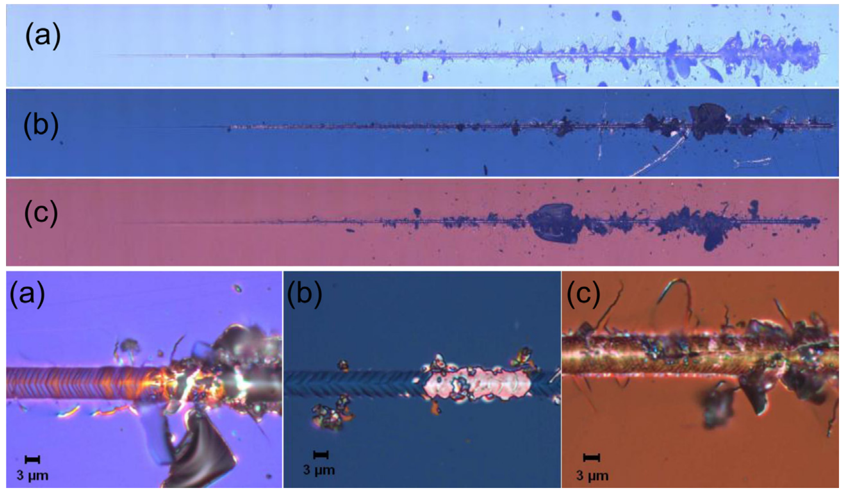

Fig. 3. (*Top*) Optical micrographs of the scratched (a) a-C:H:N/SiO$_x$, (b) a-C:H and (c) a-C:H/SiO$_x$ films. (*Bottom*) Zoom in into the full delamination area of the film for each sample. Scratch direction is from left to right.

compensation to neutralize the sample. High resolution spectra were acquired in the region of interest using the following experimental parameters: 20–40 eV energy window, pass energy of 20 eV, step size of 0.1 eV and dwell time of 1000 ms. One sweep was used to acquire all regions. The absolute energy scale was calibrated to Cu2p$_{2/3}$ peak binding energy of 932.6 eV using an etched copper plate. All spectra were calibrated to C1s peak at 284.6 eV.

3. Results and discussion

AFM 3D topographical images, normalized height distribution histograms and bearing ratio curves of characteristic a-C:H:N/SiO$_x$, a-C:H and a-C:H/SiO$_x$ surfaces obtained are shown in Fig. 1a–c, respectively. AFM 3D images show all three DLC films exhibit different morphologies with specific surface textures. Tabulated analysis of surface morphology parameters shown in Table 1 and obtained from AFM topography images provide further comparative details. All surfaces exhibited relatively low surface RMS roughness. The lowest RMS roughness of 0.73 nm was observed for a-C:H/SiO$_x$ films with the surface structures having a mean height of 2.82 nm. Largest asymmetry of surface structures was observed for a-C:H films with R_{sk} value of −0.19 which indicates a predominance of valleys. Positive skewness values were observed for a-C:H:N/SiO$_x$ and a-C:H/SiO$_x$ films indicating more surface peaks than valleys. The surface structures of a-C:H films are less random and more repetitive than on a-C:H:N/SiO$_x$ and a-C:H/SiO$_x$. Bumpy surfaces with more random and less repetitive structures were observed for a-C:H:N/SiO$_x$ films which had the lowest R_{ku} value of 4.05. Bumpy surface topography value has been reported to have a longer slip-rolling resistance (lifespan) [29].

The scratch test has been widely used for evaluation of film/substrate adhesion [30–32]. It can be regarded as a relative comparison test and is a good method for quality assurance/control testing of hard film adhesion which is useful in the process optimization of the new coatings [33]. Critical loads depend on mechanical strength (adhesion and cohesion) of the film/substrate composite, as well as on a few other parameters with some of them dependent on the test procedure itself [34]. Scratch tests were performed on all three samples with normal force, frictional force, friction coefficient, penetration depth and residual depth recorded. Fig. 2a–c shows characteristic resulting scratch parameter curves as a function of the scratch distance for a-C:H:N/SiO$_x$, a-C:H, and a-C:H/SiO$_x$ synthesized films respectively. The force applied on samples was not affected by surface topography due to the instruments force feedback loop control. These results show that a-C:H:N/SiO$_x$ films have better adhesion properties with the first delamination occurring at 24 ± 1 mN and full delamination at 134 ± 1 mN (Fig. 2a with the corresponding optical scratch image shown in Fig. 3a) while the first delamination for a-C:H/SiO$_x$ films occurs at 21 ± 1 mN and the full delamination at 131 ± 3 mN (Figs. 2c and 3c). The full delamination critical load is very similar in the case of a-C:H:N/SiO$_x$ and a-C:H/SiO$_x$ films. However, a-C:H shows differences (Figs. 2b and 3b), where the first delamination occurs at 25 ± 2 mN and full delamination at 69 ± 3 mN. From the data shown in Fig. 2, a-C:H film possesses the lowest resistance to scratching. Analysis of penetration and residual depth curves shown in Fig. 2 suggests a-C:H:N/SiO$_x$ films have better elastic recovery when compared to a-C:H/SiO$_x$ films. The increase in elastic recovery and wear resistance of the films can be associated with stronger cross-linking between graphitic planes in a-C:H:N/SiO$_x$ films and a higher degree of structural disorder [35]. Moreover, results are very reproducible as shown by the low value of standard deviation. The summary of critical load test results is presented in Fig. 4.

Although the initial surface morphology analysis and scratch data tests followed by optical inspection of the films provides quantitative information about cohesive and adhesive properties of the films, wear mechanisms in particular at the beginning of the scratching, requires some additional elucidation. AFM was used to measure critical loading sections of the scratches. AFM topographical images of L_{c1} and L_{c2} sections are presented in Fig. 5. It can be seen that the initial failure of a-C:H:N/SiO$_x$ and a-C:H/SiO$_x$ films was accomplished by a fracture according to a typical "herringbone" – style cracks [36] that appear in a scratch track (Fig. 5a and c at the L_{c1} section) due to the *fatigue + fracture* wear mechanism [37]. Compressive loading of the surface deforms it to the extent where high, mainly shear, stress is formed which exceeds the DLC film strength and the crack is formed resulting in crack growth and material detachment [37]. The same tendency could be observed for a-C:H synthesized films as "herringbone" cracks also appear on the scratch track in Fig. 2c. AFM length profile images of the L_{c1} scratch track section shown in Fig. 5a–c and optical micrographs of full film delamination for each sample in Fig. 3a–c show good qualitative agreement. However, a distinct feature of a-C:H film is more abrupt surface topography and length profile of the scratch track as compared with the other two DLC films. This difference could be attributed to the specific surface nanostructural features of a-C:H film. This can be explained as follows. During the scratch test, the indenter first has a contact with the surface peaks which fall in the upper region of the bearing ratio curve. It is suggested that scratches at a progressive load and fixed rate conditions induce very high contact stress in surface peaks resulting in DLC film crack or spall. Once the DLC film spall, the resulting wear particles could act as an abrasive material causing more damage to the film upon increased friction. The a-C:H films exhibited higher asymmetry and R_{pk} values (Table 1) which gives higher probability of the indenter meeting such peaks during the scratch path as compared with a-C:H:N/SiO$_x$ and a-C:H/SiO$_x$ films. Therefore, it is suggested that not only *fatigue + fracture* wear mechanism was present during the formation of the scratch, but also a nanostructural abrasive wear which caused stronger surface deformation and debris generation resulting in a more abrupt surface topography and earlier full delamination of the film. Additionally, another film failure could be noticed in the L_{c1} scratch track section in Fig. 5b. The scratch resembles a string of beads which indicates that some amount of the film has been displaced vertically: this may result from the high brittleness and intrinsic stress of the DLC film [38]. An AFM topographical image of the a-C:H:N/SiO$_x$ film delamination at section L_{c2} (Fig. 5a) indicates a sharp crack perpendicular to the scratch track. After this crack, adhesion between the a-C:H:N/SiO$_x$ and Cr film is broken down and full DLC film delamination takes place. Full delamination of the a-C:H film occurs abruptly with large amounts of material detached (L_{c2} scratch track section length profile in Fig. 5b) resulting in a broadening of the scratch track while full delamination of a-C:H/SiO$_x$ film (Fig. 5c) is initiated after the crack growth process when a critical amount of film have been pulled off. This shows that initial DLC film cracking mechanisms are the same for both a-C:H:N/SiO$_x$ and a-C:H/SiO$_x$ and different for a-C:H films. Furthermore, full delamination mechanisms are different for all three DLC films.

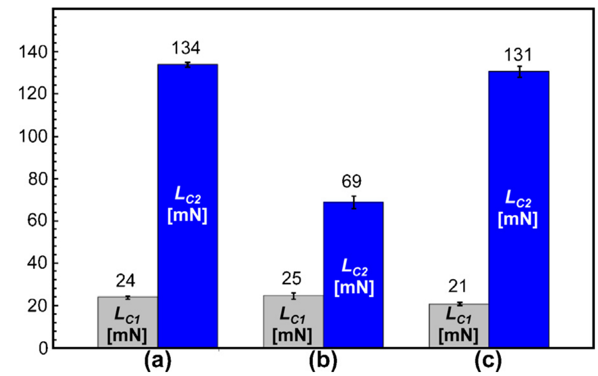

Fig. 4. Plotted summary of the critical load results of (a) a-C:H:N/SiO$_x$, (b) a-C:H and (c) a-C:H/SiO$_x$ films. L_{c1} corresponds to the first failure where the initial cracking was present and L_{c2} corresponds to the second failure at the point of the full delamination of thin films.

To gain further information, XPS analysis was performed of a-C:H:N/SiO$_x$, a-C:H, and a-C:H/SiO$_x$ films. A corresponding full elemental quantification is presented in Table 2. It can be seen that a-C:H films mostly contain carbon with some amount of oxygen present on the surface. Both a-C:H/SiO$_x$ and a-C:H:N/SiO$_x$ contained a considerable amount of silicon with 13.4 and 24.6%

Table 2
Elemental quantification obtained from XPS analysis.

Sample	C1s (%)	N1s (%)	O1s (%)	Si2p (%)
a-C:H:N/SiO$_x$	44.9	1.4	29.1	24.6
a-C:H	91.5	0.0	8.5	0.0
a-C:H/SiO$_x$	59.0	0.0	27.6	13.4

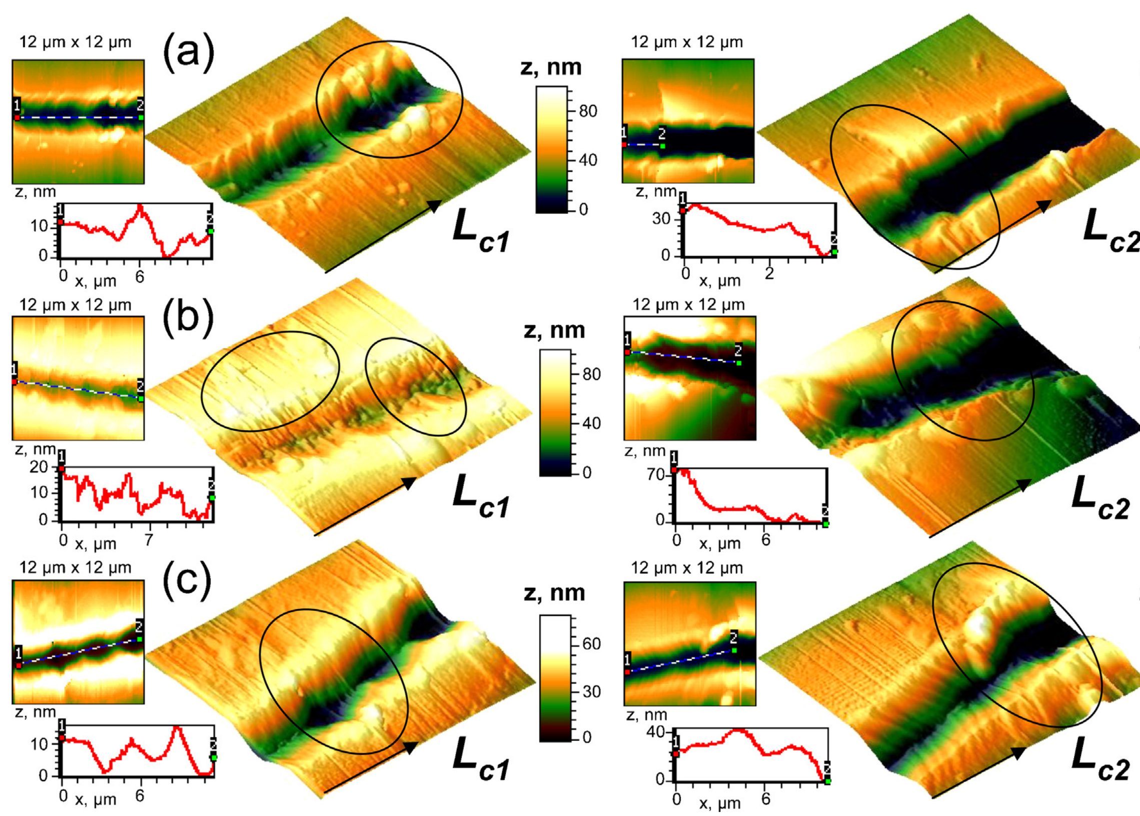

Fig. 5. Characteristic 12 μm × 12 μm AFM 3D topographical images with a normalized z scale in nm of critical loading sections along the progressive load scratch performed on of (a) a-C:H:N/SiO$_x$, (b) a-C:H and (c) a-C:H/SiO$_x$ films. Length profile images of scratch track nanostructure along the diagonal lines in AFM topographical images are also shown. The first failure L_{c1} corresponds to the initial cracking (indicated by ellipsoid markers on the topography image) while the second failure L_{c2} corresponds to the full delamination of the film (also indicated by ellipse markers). Scratch direction is indicated by a black arrow.

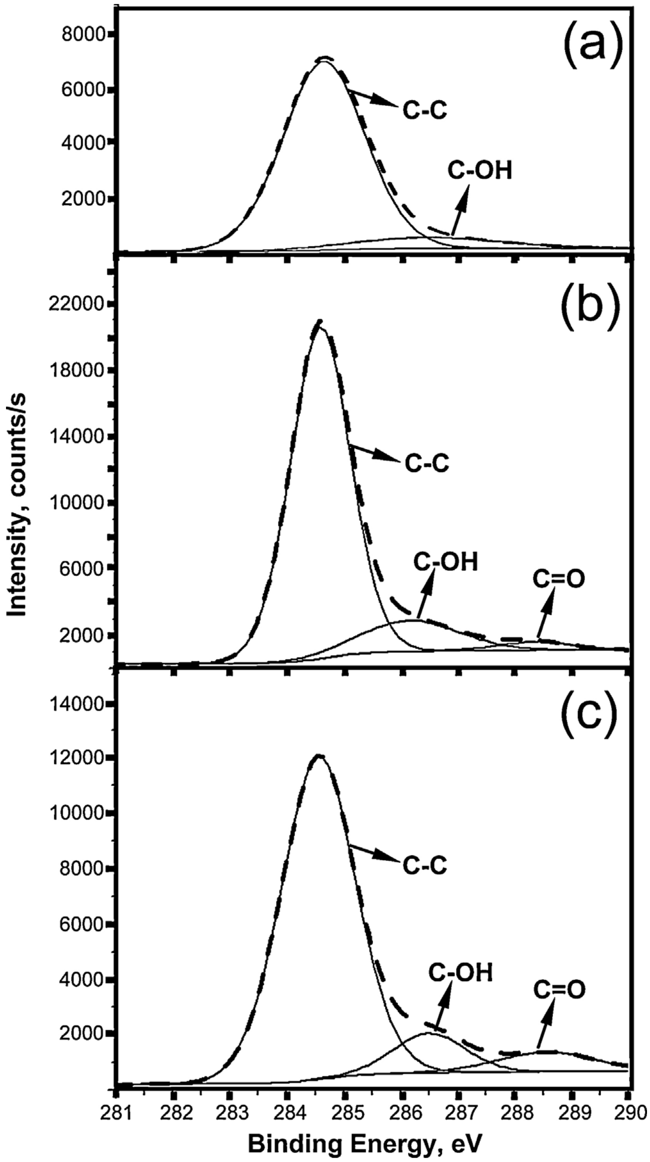

Fig. 6. High resolution C1s XPS spectra of (a) a-C:H:N/SiO_x, (b) a-C:H and (c) a-C:H/SiO_x films. Dashed lines are actual data and solid lines are Gaussian/Lorentzian product with 30% Lorentzian and 70% Gaussian character.

respectively. There is also a corresponding increase in surface oxygen presumably due to SiO_x bond formation. Additionally, while oxygen amounts remain the same between a-C:H/SiO_x and a-C:H:N/SiO_x, there is a decrease in carbon by ∼15% in the latter. This could indicate that silicon is incorporated into this film via sp^3 hybridized diamond like, not graphitic, sp^2 bonds with carbon. Alternatively, SiO_x formation and phase segregation proceeds. Similar O—Si—C bonds have been observed before in DLC films [39]. This additional amount of silicon is proposed to improve a-C:H:N/SiO_x thin film stress related properties. One can expect that use of 20% nitrogen/hydrogen mixture as carrier gas contributes to lower concentration of atomic hydrogen in the flux [19] and resultant increase of Si transfer on to the surface.

High resolution C1s XPS spectra are shown in Fig. 6 together with the corresponding peak fits. It can be seen that the major C1s peak in all three thin DLC films is due to the C—C bonds at 284.6 eV. Full width at half maximum of this peak for a-C:H:N/SiO_x, a-C:H, and a-C:H/SiO_x samples was 1.7, 1.2 and 1.5 eV, broader for both a-C:H:N/SiO_x and a-C:H/SiO_x than those typical for diamond and graphite (1.4 and 1.3 eV, respectively) [40]. It can be proposed that this is due to the carbon in both sp^3 and sp^2 bonding configurations. The exact ratio, however, cannot be accurately determined due to the absence of the distinct shoulders as well as due to the presence of Si—C—O bonds. Additionally, two more shoulders can be distinguished in a-C:H and a-C:H/SiO_x samples at 286.5 and 288.5 eV, assigned to C—O—C and O—C—O bonds respectively [40]. The latter peak was absent in C:H:N/SiO_x with the increased silicon and decreased carbon concentrations. In general, oxygenated carbon bonds have been shown to result in the decreased mechanical properties of the DLC films by terminate carbon network [41,42]. It can be proposed that the presence of nitrogen atmosphere during synthesis of DLC films decreased the amount of terminal C—O bonds thus slightly improving thin films wear resistance.

4. Conclusions

The a-C:H, a-C:H/SiO_x and a-C:H:N/SiO_x films were deposited on chromium thin film coated glass using a closed drift ion beam source and acetylene, hexamethyldisiloxane and hydrogen or 20% nitrogen/hydrogen mixture as precursors. Surface cohesive and adhesive properties of these films were investigated using progressive loading scratch tests in combination with optical microscopy as well as atomic force microscopy while elemental composition was determined using X-ray photoelectron spectroscopy. The a-C:H/SiO_x and a-C:H:N/SiO_x films showed better mechanical strength as compared to conventional a-C:H films. The a-C:H films showed a fatigue and fracture induced wear mechanism as well as additional wear due to nanostructural abrasiveness arising from the specific surface morphology of the film. X-ray photoelectron spectroscopy demonstrated increased amounts of silicon and the absence of terminal oxygenated carbon bonds which was attributed to the improved mechanical properties of a-C:H:N/SiO_x films.

Acknowledgements

This research was funded by a grant no. 31V-32 from the Agency for Science, Innovation and Technology of Lithuania. Support of Research Council of Lithuania is gratefully acknowledged. Special thanks go to Vitoldas Kopustinskas from the Institute of Materials Science of Kaunas University of Technology. Authors also gratefully acknowledge Central Microscopy Research Facility at the University of Iowa, USA, for use of XPS instrument.

References

[1] J. Robertson, Diamond-like amorphous carbon, Materials Science and Engineering Reports 37 (2002) 129–281.
[2] J. Robertson, Amorphous carbon, Advances in Physics 35 (1986) 317–374.
[3] T. Yokota, T. Terai, T. Kobayashi, T. Meguro, M. Iwaki, Cell adhesion to nitrogen-doped DLCs fabricated by plasma-based ion implantation and deposition method using toluene gas, Surface and Coatings Technology 201 (2007) 8048–8051.
[4] B. Jones, A. Mahendran, A. Anson, A. Reynolds, R. Bulpett, J. Franks, Diamond-like carbon coating of alternative metal alloys for medical and surgical applications, Diamond and Related Materials 19 (2010) 685–689.
[5] R.K. Roy, H.W. Choi, J.W. Yi, M.W. Moon, K.R. Lee, D.K. Han, J.H. Shin, A. Kamijo, T. Hasebe, Hemocompatibility of surface-modified, silicon-incorporated, diamond-like carbon films, Acta Biomaterialia 5 (2009) 249–256.
[6] S.F. Ahmed, D. Banerjee, K. Chattopadhyay, The influence of fluorine doping on the optical properties of diamond-like carbon thin films, Vacuum 84 (2010) 837–842.
[7] M. Ikeyama, S. Nakao, Y. Miyagawa, S. Miyagawa, Effects of Si content in DLC films on their friction and wear properties, Surface and Coatings Technology 191 (2005) 38–42.
[8] Y. Liu, A. Erdemir, E. Meletis, An investigation of the relationship between graphitization and frictional behavior of DLC coatings, Surface and Coatings Technology 86 (1996) 564–568.
[9] R. Hauert, A review of modified DLC coatings for biological applications, Diamond and Related Materials 12 (2003) 583–589.
[10] P. Maguire, J. McLaughlin, T. Okpalugo, P. Lemoine, P. Papakonstantinou, E. McAdams, M. Needham, A. Ogwu, M. Ball, G. Abbas, Mechanical stability,

corrosion performance and bioresponse of amorphous diamond-like carbon for medical stents and guidewires, Diamond and Related Materials 14 (2005) 1277–1288.
[11] E. Mitura, S. Mitura, P. Niedzielski, Z. Has, R. Wolowiec, A. Jakubowski, J. Szmidt, A. Sokołowska, P. Louda, J. Marciniak, Diamond-like carbon coatings for biomedical applications, Diamond and Related Materials 3 (1994) 896–898.
[12] C. Lin, D. Wei, C. Chang, W. Liao, Optical properties of diamond-like carbon films for antireflection coating by RF magnetron sputtering method, Physics Procedia 18 (2011) 46–50.
[13] V. Litovchenko, N. Klyui, Solar cells based on DLC film–Si structures for space application, Solar Energy Materials and Solar Cells 68 (2001) 55–70.
[14] B. Gupta, B. Bhushan, Micromechanical properties of amorphous carbon coatings deposited by different deposition techniques, Thin Solid Films 270 (1995) 391–398.
[15] B. Bhushan, S. Sundararajan, Micro/nanoscale friction and wear mechanisms of thin films using atomic force and friction force microscopy, Acta Materialia 46 (1998) 3793–3804.
[16] Š. Meškinis, R. Gudaitis, V. Kopustinskas, S. Tamulevičius, Electrical and piezoresistive properties of ion beam deposited DLC films, Applied Surface Science 254 (2008) 5252–5256.
[17] Y. Kim, S. Cho, W. Choi, B. Hong, D. Yoon, Dependence of the bonding structure of DLC thin films on the deposition conditions of PECVD method, Surface and Coatings Technology 169 (2003) 291–294.
[18] A. Tamulevičienė, Š. Meškinis, V. Kopustinskas, S. Tamulevičius, Diamond like carbon film as potential antireflective coating for silicon solar cells, Materials Science = Medžiagotyra/Kaunas University of Technology, Academy of Sciences of Lithuania. Kaunas: Technologija (2010), ISSN 1392-1320.
[19] A. Tamulevičienė, Š. Meškinis, V. Kopustinskas, S. Tamulevičius, Carrier gas and ion beam parameter effects on the structure and properties of a-C:H/SiO_x films deposited employing closed drift ion beam source, Nuclear Instruments and Methods in Physics Research B 282 (2012) 116–120.
[20] Y. Pauleau, Residual stresses in DLC films and adhesion to various substrates, in: Tribology of Diamond-like Carbon Films. Fundamentals and Applications, Springer, New York, USA, 2008102–136.
[21] C. Wei, J.Y. Yen, Effect of film thickness and interlayer on the adhesion strength of diamond like carbon films on different substrates, Diamond and Related Materials 16 (2007) 1325–1330.
[22] Y. Funada, K. Awazu, H. Yasui, T. Sugita, Evaluation of raw hardness of DLC thin films prepared by IBAD, Nuclear Instruments and Methods in Physics Research B 148 (1999) 664–668.
[23] A. Stalder, G. Kulik, D. Sage, L. Barbieri, P. Hoffmann, A snake-based approach to accurate determination of both contact points and contact angles, Colloids and Surfaces A 286 (2006) 92–103.
[24] A. Lazauskas, V. Grigaliūnas, F. Ecarla, M. Caunii, A comparative evaluation of surface morphology, cohesive and adhesive properties of one-step and two-step thermal deposited chromium thin films on glass substrates, Applied Surface Science 258 (2012) 7633–7638.
[25] A. Tamulevičienė, Š. Meškinis, V. Kopustinskas, S. Tamulevičius, Multilayer amorphous hydrogenated carbon (aC:H) and SiO_x doped aC:H films for optical applications, Thin Solid Films 519 (2011) 4004–4007.
[26] N. Tayebi, A. Polycarpou, Adhesion and contact modeling and experiments in microelectromechanical systems including roughness effects, Microsystem Technologies 12 (2006) 854–869.
[27] M. Sedlaček, L.M. Silva Vilhena, B. Podgornik, J. Vižintin, Surface topography modelling for reduced friction, Strojniski Vestnik: Journal of Mechanical Engineering 57 (2011) 674–680.
[28] N. Randall, G. Favaro, C. Frankel, The effect of intrinsic parameters on the critical load as measured with the scratch test method, Surface and Coatings Technology 137 (2001) 146–151.
[29] D. Spaltmann, M. Löhr, S. Binkowski, M. Woydt, Einfluss der Topographie von DLC-Schichten auf deren Verhalten unter geschmierter Wälzbeanspruchung, Tribologie und Schmierungstechnik 51 (2004) 18–26.
[30] A. Perry, The adhesion of chemically vapour-deposited hard coatings to steel – the scratch test, Thin Solid Films 78 (1981) 77–94.
[31] H. Hintermann, Adhesion, friction and wear of thin hard coatings, Wear 100 (1984) 381–397.
[32] S. Bull, D. Rickerby, New developments in the modelling of the hardness and scratch adhesion of thin films, Surface and Coatings Technology 42 (1990) 149–164.
[33] S. Bull, E. G-Berasetegui, An overview of the potential of quantitative coating adhesion measurement by scratch testing, Tribology and Interface Engineering Series 51 (2006) 136–165.
[34] P. Steinmann, Y. Tardy, H. Hintermann, Adhesion testing by the scratch test method: the influence of intrinsic and extrinsic parameters on the critical load, Thin Solid Films 154 (1987) 333–349.
[35] W. Gammon, G. Hoatson, B. Holloway, R. Vold, A. Reilly, Bonding in hard and elastic amorphous carbon nitride films investigated using {15}N, {13}C, and {1}H NMR spectroscopy, Physical Review 68 (2003) 195401.
[36] G.D. Vaughn, B.G. Frushour, W.C. Dale, Scratch indentation, a simple adhesion test method for thin films on polymeric supports, Journal of Adhesion Science and Technology 8 (1994) 635–650.
[37] K. Holmberg, H. Ronkainen, A. Laukkanen, K. Wallin, Friction and wear of coated surfaces – scales, modelling and simulation of tribomechanisms, Surface and Coatings Technology 202 (2007) 1034–1049.
[38] L.Y. Huang, J.W. Zhao, K.W. Xu, J. Lu, A new method for evaluating the scratch resistance of diamond-like carbon films by the nano-scratch technique, Diamond and Related Materials 11 (2002) 1454–1459.
[39] L. Randeniya, A. Bendavid, P. Martin, M.S. Amin, E. Preston, Molecular structure of SiO_x-incorporated diamond-like carbon films; evidence for phase segregation, Diamond and Related Materials 18 (2009) 1167–1173.
[40] X. Yan, T. Xu, G. Chen, S. Yang, H. Liu, Study of structure, tribological properties and growth mechanism of DLC and nitrogen-doped DLC films deposited by electrochemical technique, Applied Surface Science 236 (2004) 328–335.
[41] H. Li, T. Xu, C. Wang, J. Chen, H. Zhou, H. Liu, Friction behaviors of hydrogenated diamond-like carbon film in different environment sliding against steel ball, Applied Surface Science 249 (2005) 257–265.
[42] H. Li, T. Xu, C. Wang, J. Chen, H. Zhou, H. Liu, Friction-induced physical and chemical interactions among diamond-like carbon film, steel ball and water and/or oxygen molecules, Diamond and Related Materials 15 (2006) 1228–1234.